CrossMark

Handling interference in self-organizing femtocell networks through frequency-polarization diversity

Ponnu Jacob[1] · A. S. Madhukumar[1]

Abstract The next generation heterogeneous networks are expected to offer higher data-rate and better QoS to the customers by leveraging smaller cells like femtocells and making use of orthogonal frequency division multiple access. However, uncoordinated dense deployment of femtocells in macrocell network pose unique challenges involving cross-tier interference and resource management which results in significant degradation of the system performance. As part of addressing these challenges for the successful integration of both technologies, this paper proposes the deployment of a self-organizing femtocell network that employs an opportunistic smart frequency reuse technique –cross polarized complementary frequency allocation (CPCFA). It exploits the frequency and polarization diversity to mitigate interference in two-tier femto-macro networks. In this work, a strategy combining the adoption of reverse frequency allocation and orthogonal polarized transmission is analyzed as a potential solution for maximizing spectral efficiency and minimizing interference in the existing heterogeneous networks. Focus of the current work is on downlink transmission where the traffic is high and the deployment of femtocell is more beneficial. The results of analytic and simulation studies prove that CPCFA increases the scope for an easily implementable, remarkable opportunity in the context of two-tier femto-macro network that can substantially increase the system capacity as well as cell coverage without additional network complexities.

1 Introduction

Explosive demands for high data-rate communication networks with better spectral efficiency is the key driving force towards continued technology evolution in the field of wireless communication. Also, with proliferation of various multi-media devices, future wireless access networks are expected to be autonomous in terms of operation. Hence, they should exhibit a significant degree of self-organization and self-optimization characteristic as also recognized by the standardization body-3rd Generation Partnership Project (3GPP) [1]. These objectives can be achieved by combining advances in communication technology, smart topology design, and spectrum reframing [2]. As the most effective step towards addressing these challenges, self-organizing femtocells with 'easy plug and play property' have been recently gaining significant attention. Currently, 3GPP LTE-Advanced and IEEE 802.16 m are standardizing the self-organizing network concept for IMT-Advanced femtocell networks as well [3–7]. Moreover, considering the volume of traffic that is expected in the future years, the convergence of optic fiber backhauls to radio over fiber backhauls is quite promising in the case of heterogeneous networks [8].

The co-existing architecture of macrocell network along with self-organizing femtocells hold the potential in meeting high data-rate demands which enable the network operator in accommodating more traffic. However, the

✉ Ponnu Jacob
ponnu1@e.ntu.edu.sg

A. S. Madhukumar
ASMadhukumar@ntu.edu.sg

[1] Nanyang Technological University, Nanyang Avenue, Singapore 639798, Singapore

deployment being highly dense and planned by the user themselves, restricts the control of user on the topology and activity of the femtocell. As a result, conventional network planning, configuration and optimization for femtocell networks is quite a difficult task [3]. The different tiers of the femto-macro network share the same frequency channels or orthogonal ones so as to avoid the need for a new user equipment which ends up in cross-tier interference. Hence, the interference between two tiers should be managed through proper frequency allocation schemes, which allow efficient utilization of the scarce radio spectrum and assure the highest level of user's quality of experience [4]. Although the interference in a femto-macro network cannot be fully eliminated, it is possible to limit it within a reasonable range by smarter resource management. For the same reason, the resource management solutions for femtocells cannot be separated from the macrocell and is difficult to be designed from scratch. This motivates the introduction of self-organization characteristic into the femtocells. This helps it to intelligently access the macrocell spectrum and thereby reduce the operational expense and subscriber churn by eliminating any human involvement in the network configuration process. Even though several methods of self-organization [5–7] which alleviates the macro-femto interference [9], are available in the literature, self-organizing femtocells that promote orthogonal resource allocation between two-tiers has not drawn much attention and forms the main focus of this work.

The current challenges of capacity crunch and limited coverage in wireless networks can no longer be addressed by increasing the base station density alone. This further encourage the researchers to design better frequency reuse techniques, orthogonal spectrum allocation and alignment techniques. To address these problems, extensive research is being carried out in the field of self-organizing, cognitive femtocells [10–11]. They are capable of autonomously integrating into the cellular framework and the benefits are reflected more with colossal increase in base station density. Since the selection of an interference management strategy relies on the trade-off between complexity and efficiency that it offers, fractional frequency reuse is considered as an optimal choice mainly due to its marginal complexity and minimal signaling overhead. It has also proved to enhance the system throughput by a large margin while maintaining the QoS demands to the customers. Broad comparison of different interference management and frequency reuse techniques are analyzed in [12], which finally proposes the optimal static fractional-frequency allocation (OSFFA) as the one that offers superior performance in heterogeneous networks. In addition to this architecture, improving the orthogonal characteristics of frequency carriers and efficient reuse of available spectrum

can further enhance the system performance. It is in this context, that we propose an OFDM transmission system for self-organizing femtocells embedded in a macrocell network. It incorporates the concept of reverse frequency allocation [13, 14] within an orthogonally polarized transmission network [15, 16]. Exploiting both frequency and polarization diversity helps in improving the system performance by effectively controlling the cross-tier interference and efficiently managing the radio spectrum. In RFA, the femtocells adopt the reversed order of uplink (UL) and downlink (DL) frequencies used by the macrocell network for its transmission, in addition to a well-planned geographical separation. This better balances the requirements of higher spectral efficiency and reduced inter-cell interference. Furthermore, femtocells and macrocells make use of orthogonal polarization for transmission to ensure isolation between the two networks and thereby reduce interference. This further enables the same frequency carrier to be used simultaneously by both networks in the same location. These strategies coupled in a self-organizing femtocell network guarantees capacity maximization and interference minimization through increased signal to interference plus noise ratio (SINR) and dynamic spectrum access which eventually makes it a potential candidate for adoption in the next generation cellular architectures.

The rest of the paper is organized as follows. Section 2 discuss the motivation behind the adoption of CPCFA strategy along with the detailed description of related works on how spatial separation and frequency isolation can contribute towards efficient interference mitigation. Section 3 projects the CPCFA framework in detail. Section 4 carries out the system analysis which is further used in the extensive simulations in Sect. 5. Section 6 finally concludes the paper.

2 Related works

2.1 Reverse frequency allocation

In classical macrocell network which operates in FDD mode, UL and DL transmissions take place along two separate bands which are allocated in pair to every single user. However, in a co-existing femto-macro network, the DL/UL transmission from the macrocell can interfere with the DL/UL transmission of the femtocell if both of them transmit along the same frequency band simultaneously. Hence, a potential solution to avoid interference is to prevent femtocell and macrocell from using the same frequency band for simultaneous transmission whether it be in UL or DL in the same location. However, scarcity of the highly expensive spectral resources prohibit the femtocell and macrocell from using dedicated spectrum for transmission

as it results in spectral inefficiency. An easy and implementable approach is to reverse the UL and DL transmissions between femtocell and macrocell network [13]. This kind of complementary spectrum allocation between femto-macro network for UL and DL transmission prevents one network from interfering with the other during their transmissions. Further, in order to prevent the UL transmission of the macrocell users interfering with the DL transmission of the femtocell users and vice versa, geographical separation is also employed during spectrum allocation. The main advantage of this "Reversed Mode" spectrum allocation is that, it neither needs a dedicated spectrum for femtocell operation, nor does it consume the macrocell spectrum. However it doubles the spectral efficiency when compared to that of OSFFA scheme. This is because the entire macrocell spectrum $(S_1 + S_2)$ is made available to the femtocells but the UL and DL frequencies are interchanged/reversed $(S'_1 + S'_2)$ in the femtocell operation to ensure minimal interference as demonstrated in Fig. 1.

2.2 Cross polarized transmission

Classical wireless communication systems have relied on one channel per frequency, although it is well understood that two polarization states of plane waves allow two distinct information channels. Techniques such as 'polarization diversity' already take advantage of this. Polarization diversity can be used as a tool to exploit frequency diversity by assuring minimal co-channel interference by virtue of its property known as cross polarization discrimination (XPD). XPD is defined as the ratio between the temporal-average power in the emitted polarization and the value of temporal-average power that has leaked into other polarization [17]. XPD represents the polarization state of a wireless signal. In a transmission channel, maximum signal

strength between nodes occur when both transmitter and receiver use identical polarization. However, due to XPD, when a given antenna receives a co-channel signal sent from a cross-polarized antenna, the effective signal strength is reduced by several dB. Larger the XPD between polarized transmissions, larger will be the isolation. The two distinct polarization modes of a dual-polarized wireless channel being co-polar (represented by ||) and cross-polar (represented by ⊥), XPD of a co-polar signal whose power is $P^{||}$ is given by:

$$XPD_{||} = \frac{P^{||}}{P^{(||\rightarrow\perp||)}} \quad (1)$$

and that of a cross-polar signal whose power is $P^{\perp}$ is given by :

$$XPD_{\perp} = \frac{P^{\perp}}{P^{(\perp\rightarrow||)}} \quad (2)$$

where $P^{(||\rightarrow\perp)}$ and $P^{(\perp\rightarrow||)}$ represent the amount of power that has leaked from co-polar channel to cross-polar channel and vice versa respectively. Hence, in order to avoid interference between the two-tiers, orthogonality in signal polarimetric dimension is employed. The polarization of both networks being orthogonal to each other due to their sense of rotation as in Fig. 2, assures isolation between them which helps in interference reduction and hence improve the SINR. At this point, a significant challenge to be addressed is to choose between the different type of polarization for wireless signal transmission-linear (includes vertical and horizontal) or circular (right-hand and left-hand). Definitely linear polarization has an edge over circular polarization in terms of expense and ease of implementation. However, these advantages do not stand valid in case of a mobile ad-hoc environment, where the user equipment (UE) is not stationary and variations in
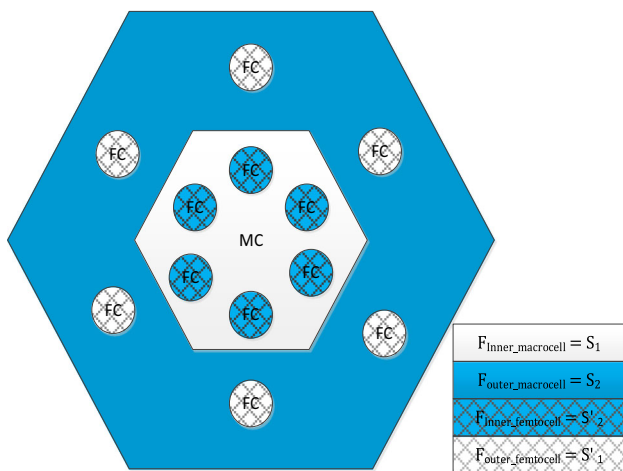

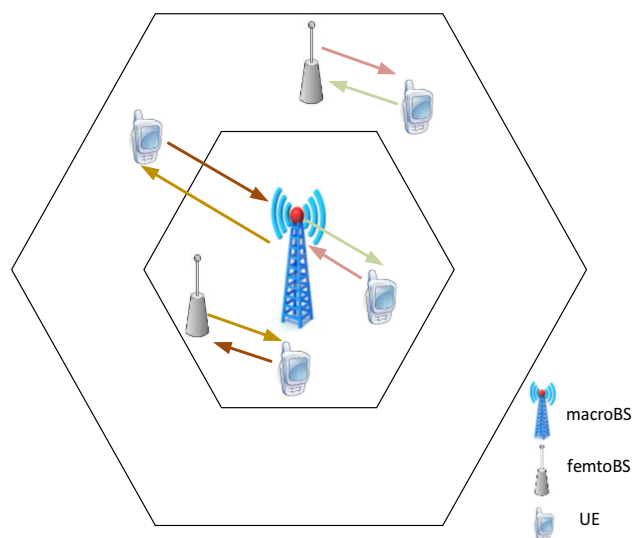**Fig. 1** Reverse frequency allocation strategy

$F_{Inner\_macrocell} = S_1$
$F_{outer\_macrocell} = S_2$
$F_{Inner\_femtocell} = S'_2$
$F_{outer\_femtocell} = S'_1$

Fig. 2 Cross-polarized transmission in femto-macro network

macroBS
femtoBS
LHCP
RHCP
UE

polarization alignment is possible. The advanced signal propagation properties enable the circular polarization antenna technology to offer numerous performance advantages over traditional linear polarized technologies. Circular polarization helps in effectively addressing all the challenges incurred in the conventional linear transmission. It does not incur phasing issues and is capable of establishing reliable signal links regardless of the antenna orientation of the device. It is much better at penetrating obstructions and the signal is not adversely impacted by obstructions and other environmental conditions. Unlike the linear polarized antennas, transmission takes place along all planes in a circular polarized transmission which lowers the likelihood of signal cancellation and is hence suitable for use in non-line-of-site applications. The recent past breakthrough in antenna design and innovative scientific burst outs have made this technology affordable for common applications as well. The analysis of polarization effects in indoor wireless high data-rate communication scenarios in [18] claims that appropriate use of circular polarization could lead to significantly reduced channel delay spread, and hence improved error performance even with minor attenuation. In addition to this [19] shows that the variation of rms delay spread as a mobile moves over several wavelengths is also greatly reduced when circular polarized antennas are used. Extensive simulations and analysis carried out in [20–21] approves that the use of circular polarization is advantageous in reducing the effects of multipath delays and reflections from the wall even when it has a multi-layered structure. Above all, the significant advantage of circular polarization is that even after multiple reflections, refractions and delay, its sense of rotation can never be altered by any naturally existing substance even though there can be a minor shift in angular orientation. This assures that orthogonality is always maintained between two tiers of the network.

3 Cross polarized complementary frequency allocation strategy

With billions already spent, network operators always search for effective methods to squeeze out the maximum out of the existing multi-tier networks. In these networks, when one of the tier is unplanned and uncoordinated, the key challenge of allocating scarce spectral resource to the users should be addressed effectively [22]. As we know, both higher cross-tier interference (with shared spectrum usage) and limited spectrum availability (with dedicated spectrum usage) are capacity-limiting factors. Hence, Cross-Polarized Complementary Frequency Allocation (CPCFA) strategy is designed by incorporating the merits of the aforementioned methods in Sect. 2, where frequency

diversity along with polarization diversity is exploited to improve the system performance. For this purpose, we consider a macrocell network with an operator-planned static frequency allocation having a frequency reuse factor of 1, within which self-organizing femtocells are embedded. These femtocells are capable of dynamic spectrum access by exploiting the CPCFA strategy. Here, the self-organizing femtocell base station (femtoBS) sense the user operations in its vicinity which enables it to take real-time decisions regarding its operational spectrum. They are aware of the nearby user actions and future intensions via inter-cell communication enabled through femtocell gateways, or femtoBS assisted sensing. It takes input from the nearby macrocell base station (macroBS) based on which it configures its own operational frequency. The aim is to minimize the interference that it cause to users in its vicinity. Then comes the self-optimization, where the femtocell management system (FMS) reconfigures the spectrum allocation in order to satisfy the QoS demands of subscribers through optimal sub-carrier allocation and cross-polarized orthogonal transmission. It also maximizes the spectrum access of femtocell in times of heavy user traffic within each zone of the macrocell. Above all, it takes care of the self-healing part, where it switches its operational frequency or initiates a handover in times of intolerable co-tier interference. In essence, even with scarcity in the available radio spectrum, it is the self-organizing femtocell that operates on reverse frequency strategy, that enables the two tier network to achieve better spectral efficiency. Also the femtocell nodes carry out transmission via right hand circular polarized (RHCP) signals which is orthogonal to that of left hand circular polarized (LHCP) transmission used by macrocell nodes.

Fig. 3 Reverse Frequency Allocation for a single cell

This support independent operation across tiers by exploiting polarization diversity with two senses of rotation.

Figure 3 demonstrates the crucial idea behind the CPCFA strategy where a macrocell coverage area is initially partitioned into two non-overlapping regions namely the cell-center (inner region) and cell-edge (outer region). The total available macrocell spectrum is also partitioned and allocated to these two regions which is then reversed and allocated to the femtocells located within these alternate regions. Depending on whether the user belongs to the femtocell network or the macrocell network, the polarization mode for transmission is further chosen between LHCP for macrocell and RHCP for femtocell. This spectrum partitioning and the reverse frequency allocation for a single cell is depicted in Fig. 4.

However, the spectrum allocation using CPCFA strategy is not that simple in case of a multi-cell scenario which needs to be wisely formulated in order to facilitate flexibility, scalability and higher efficiency. It should ensure that both macrocell and femtocell are benefited in terms of better capacity, lower interference and higher spectral efficiency. For this purpose, the femtocells must be capable of self-configuring its resource utilization and optimize its usage in accordance with the system parameters at run-time [23]. There is a series of steps involved to satisfy this criteria. Hence, the following procedures explain the operation of CPCFA strategy in a three-cell cluster which can be further scaled to any number of cells in the network. Further in our studies, the user equipment registered to macroBS are referred to as macroUEs and those registered to femtoBS are referred to as femtoUEs.

3.1 Location cognizance for macroUEs

The macrocell spectrum allocation is methodically planned by the network operator. As a result, the task of partitioning the macrocell coverage area, into two non-overlapping regions namely the cell-center (inner) and the cell-edge (outer) region is also carried out by the network operator.
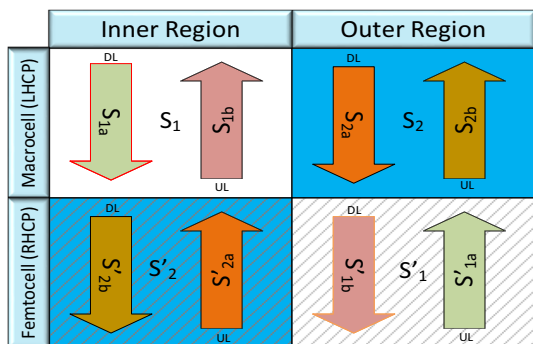

Fig. 4 Frequency distribution for a single cell in CPCFA method

However, the radius of the cell-center region is a significant design parameter which may be dependent on the user density, QoS requirement of the customers, spectrum resource availability etc. To aid this decision making, it was shown in [24] using Monte Carlo simulations that, the average network capacity is maximized for uniformly distributed UEs, if the cell-center region radius is 0.65 times the macrocell radius. The same channel allocation and cell-center region radius is adopted in our analysis as well. Thus macroBS identifies the macroUEs located within 65 % of its radius as inner region macroUEs and those outside as outer region macroUEs. This partitioning is dependent on specific multipath and fading profiles which is neglected in our studies for fair comparison.

3.2 Spectrum allocation for the macrocell

Sectorization in the cellular network diminishes the need for new macrocell sites. At the same time, operators get superior capacity and to a lesser extend better coverage without densification of the macrocell network. Hence every macrocell which is partitioned into cell-center and cell-edge region is further sub-divided into six sectors as shown in Fig. 5. The total available bandwidth (S) of the macrocell is divided into OFDMA time–frequency units and allocated to the inner region (S_1) and outer region (S_2) macroUEs such that $S = S_1 \cup S_2$. This means that the partition S_1 contains the UL and DL frequency carriers for the inner region macro-users whereas the partition S_2 contains the UL and DL frequency carriers for the outer region macro-users. Here (S_1) contains a major portion of the total available carriers which is allocated to the cell-center region or the inner region (C1–C6) macroUEs by the network operator and is named as sub-band A. The cell-edge (outer) region spectrum (S_2) is further sub-divided into six sub-bands B, C, D, E, F, G and allocated to cell-edge region (E1–E6) macroUEs as in Fig. 5. In short, frequency reuse factor (FRF) of 1 is applied to the cell-center region and FRF of 6 is applied to the cell-edge region resulting in the entire macrocell to embrace an FRF of 1. Thus, the macrocell employs static spectrum allocation meticulously planned by the network operator, which also assures the absence of intra-cell interference due to the OFDMA technology adopted. Here the boundaries of every single zone is neither rigid nor of uniform geographical size or shape as depicted in the figure, due to fading. It merely highlights the need for a spatial separation in resource allocation so as to enable spectrum reuse without interfering each other's operation. It also highlights that, the cell-center region macroUEs do not reuse the spectrum of the cell-edge region macroUEs, as a result of which the entire macrocell system is free from inter-cell interference. The use of distributed antenna system (DAS) [25] supports
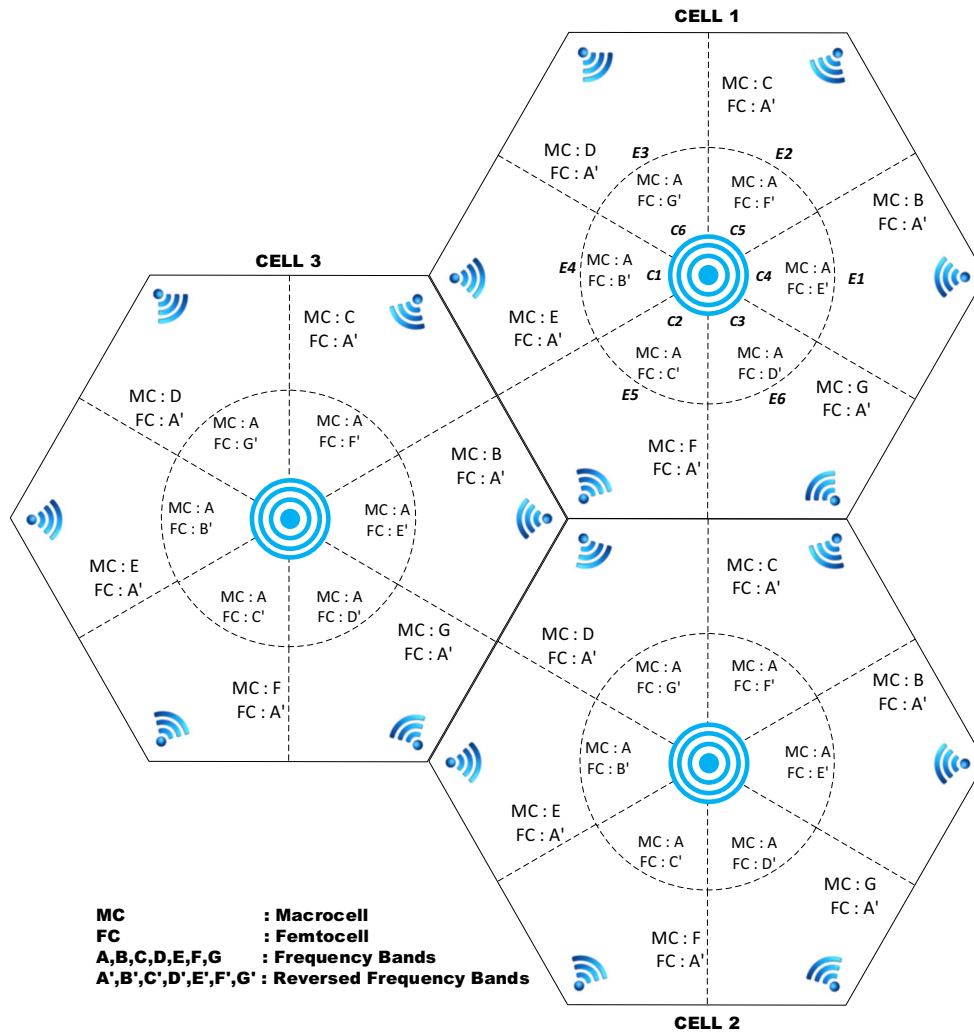
Fig. 5 Femtocell spectrum selection in CPCFA based on macrocell spectrum allocation

this mode of sectored spectrum allocation along with spatial frequency reuse within the macroBS coverage area. The radio transmission in the cell-center region is carried out by a centrally located macroBS with omni-directional antenna which holds the main processing modules like the channel cards. For the cell-edge region, we resort to the distributed antenna elements. The DAS in our proposed architecture constitute the central macroBS and 6 directional distributed antenna elements (DAE) connected through high-speed back bone network. With proper configuration and planned positioning of DAEs, DAS has the potential for outperforming centralized antenna system due to which the location decision of DAE is important. Hence the directional DAEs are 120° directional antennas, each located at the vertex of the cell, facing towards the central macroBS as shown in Fig. 5 [26]. Taking DAS into consideration, the partitioning in Fig. 5 can be perceived as the average coverage footprints of the multiple antenna elements over a period of time. DAS is also capable of

optimizing the transmission characteristics by ensuring proper tilt angle for the antenna which has a direct influence on the coverage and interference parameters of the network. Down tilting along with accurate beam forming of the antenna reduces interference to neighbors but increases capacity of the nearby users, whereas up tilting increases the coverage. The major motive behind deploying DAS is to avoid the location optimality problem which can be annoying in case of real cellular systems. The other reason being inter-cell interference mitigation through reduced transmit power which boosts the system capacity and offer better coverage mainly due to the absence of overlapping frequency bands. In our work, the connection between the macroBS and the DAEs is through optical fiber, so that the assumption of near-perfect reception of data at the DAE from the macroBS becomes realistic. However, it should be noted that, the interference—free low cost implementation of such a multi-tier system with all these benefits come at the cost of an additional system complexity.

3.3 Location cognizance for femtoUEs

Femtocells are plug and play devices which are installed by the customers without any prior planning. Unlike the macrocells, they can be turned on and off at any time, making their deployment completely random. Hence the position and location of the femtocells within the macrocell vary continuously. As a result, femtoBS needs to sense the environment and be aware of its own location as well as its neighbors in the macrocell coverage area. However, the radio transmission range between the femtoBS and the femtoUE is comparatively small. Hence we assume that the femtoUE lies within the same zone as that of the femtoBS. In short, similar to the macroUEs, femtoBSs and hence femtoUEs are also classified based on their location.

Since, femtocells are usually located indoors, the registered physical address associated with the broadband IP address or the GPS location information obtained during its installation can be used as a measure to assist the location selection. Assuming the femtocell to be stationary for a long period of time after being deployed, its position can be tracked when it locks to a GPS signal to ensure that its area of operation is legal to transmit along a specific band. Since the frequency planning does not require any real-time feedback and assuming that the femtocells are immobile after deployment, their GPS information obtained via femtocell-gateway assists in tracking its location.

Now RFA is employed and hence the spectrum allocated to macroUEs is reversed and assigned to the randomly distributed femtoUEs based on their location i.e. the frequency spectrum of the cell-center region macroUEs (S_1) is allocated to the femtoUEs in the cell-edge region and that of the cell-edge region macroUEs (S_2) is allocated to the cell-center region femtoUEs. In essence, the spectrum partitions S_1' and S_2' of femtocell correspond to the reversed UL and DL frequency pairs of spectrum partitions S_1 and S_2 of macrocell respectively. However, sectorization and geographical separation is applicable to femtoUEs as well, in case of a three cell cluster which is explained in the next section.

3.4 Spectrum selection by femtoUEs (self-configuration)

Though the macrocell depends on static spectrum allocation with unity frequency reuse factor, the massive deployment of femtocells demand more spectral resources which encourage the adoption of dynamic spectrum access. As a result, the operation of femtocells is expected to be self-organizing with an autonomous spectrum selection process. The self-organization mechanism includes self-configuration and self-optimization phases. Self-configuration is the phase soon after the femtoBS is switched

on, in which the femtoBS within each sector configures its own operational frequency based on the input that it senses from the neighboring macrocell environment. It selects the least interfering sub-band for its operation along which it transmits in the reverse mode with a polarization orthogonal to that of the macrocell transmission.

The sectorization process and the corresponding frequency band selection by the femtoBSs is summarized in Stage 1 of operational algorithm furnished in Table 1. In the self-configuration phase, each femtoBS select its operational frequency among the N available sub-bands. Let F_o and F_i represent the number of femtocell users in the outer and inner region respectively whereas M_o and M_i represent the number of macrocell users in the outer and inner region respectively. Firstly, similar to the methodology in [27], the set of usable frequency sub-bands S_f for the femtoBS j is initialized to the set of all frequency sub-bands S made available to the macroBS, where $S = S_{Mi} \cup S_{Mo}$. Here S_{Mi} is the frequency spectrum available to the inner region macroUEs and S_{Mo} is the frequency spectrum available to the outer region macroUEs. Several wireless communication standards have highlighted the capability of wireless nodes in sensing and measuring the instantaneous signal strength (RSSI) for all sub-carriers [28–30]. Hence, as the femtoBS j is switched on, it senses the radio signals received from the neighboring macroBS and estimates the RSSI value R_f for each received frequency sub-band. Let R_x denotes the RSSI value for a sub-band say x and R_f^* denote the highest RSSI value. Analyzing the strength of the received signals, if the RSSI value of sub-band A is found to be the highest, it means that femtoBS j is located in the cell-center region i.e. within any of the six sectors C1–C6 as in Fig. 5. In this case, femtoBS j forms S_f^*, a set of six sub-bands among the pack of seven sub-bands, whose signal strength received at femtoBS j is comparatively higher. The set S_f^* is now excluded from S which leaves behind the 7th sub-band to be allocated to femtoBS j in the reversed mode. If the RSSI value of sub-band A is not the highest, then it means that femtoBS j is located in the cell-edge region within any of the six zones represented by E1-E6. In this case femtoBS forms S_f^* which comprises of the set of all sub-bands except A. Excluding S_f^* from S results in sub-band A to be allocated to femtoBS j in the reversed mode (A').

With reference to the static spectrum allocation adopted for the macrocell, Fig. 5 depicts the best possible sub-bands for femtocell operation in each zone during the first iteration of the algorithm owing to minimal interference. Since the macrocell radio transmission range for sub-band A is restricted to the cell-center region, the femto-user equipments (femtoUEs) will make use of sub-band A' in the cell-edge region owing to least interference

Table 1 Algorithm for CPCFA in 3 cell cluster

Algorithm 1: Operational Algorithm for sub-carrier selection in CPCFA scheme

----

1: *Stage 1*
2: ∀ RHCP femtoBS $j \in (F_o U F_i)$ **do**
3: $\quad\quad S_f \quad \leftarrow S$ $\quad\quad\quad\quad\quad\quad\quad\quad\quad$ {Initialization}
4: $\quad\quad N_i, N_o \leftarrow N$ (Total no: of sub-bands = 7)
5: $\quad\quad R_x \quad\quad \leftarrow$ RSSI values for sub-band x
6: $\quad\quad R_f^* \quad\quad \leftarrow$ Highest RSSI value for a sub-band at femtoBS j
7: $\quad\quad$ **if** $(R_f^* = R_A)$ **then** $\quad\quad\quad\quad$ {femtoBS j is located in the cell-center region}
8: $\quad\quad\quad\quad S_f^* \leftarrow$ Set of (N-1) sub-bands with comparatively higher RSSI value
9: $\quad\quad\quad\quad S_{fi} \leftarrow S_f - S_f^{*}{}'$ $\quad$ {frequency sub- band allocated for femtoBS j}
10: $\quad\quad$ **else** $\quad\quad\quad\quad\quad\quad\quad\quad\quad\quad\quad$ {femtoBS j is located in the cell-edge region}
11: $\quad\quad\quad\quad S_f^* \leftarrow$ Set of all sub-bands except A
12: $\quad\quad\quad\quad S_{fo} \leftarrow S_f - S_f^{*}{}'$ $\quad$ {frequency sub-band allocated for femtoBS j}
13: $\quad\quad$ **end if**
14: *Stage 2a* $\quad\quad\quad\quad\quad\quad\quad\quad$ {no-more free sub-carriers in current inner region sub-band}
15: $\quad\quad\quad$ **while** $(S_{fi} = NULL, N_i \ not\ equal\ 0)$ **do**
16: $\quad\quad\quad\quad\quad N_i \quad \leftarrow \ N_i-1;$
17: $\quad\quad\quad\quad\quad S_{fi} \leftarrow (S - S'_{fi})$
18: $\quad\quad\quad\quad\quad S_f^* \leftarrow$ Set of (N_i-1) sub-bands with comparatively higher RSSI value
19: $\quad\quad\quad\quad\quad S_{fi} \leftarrow S_{fi} - S_f^{*}{}'$ $\quad$ {frequency sub- band allocated for femtoBS j}
20: $\quad\quad\quad\quad\quad$ **if** $(SINR_{UL\_Fi}$ at femtoBS j on occupied sub-carrier within $S_{fi} < T$ for $t > \tau_l)$ **then**
21: $\quad\quad\quad\quad\quad\quad\quad$ Decrease transmit power of femtoUE attached to femtoBS j by δ
22: $\quad\quad\quad\quad\quad$ **end if**
23: $\quad\quad\quad\quad\quad$ **if** $(SINR_{UL\_Fi}$ at femtoBS j on occupied sub-carrier within $S_{fi} < T$ for $t > \tau_2)$ **then**
24: $\quad\quad\quad\quad\quad\quad\quad$ **if** (interfering femtoUE within coverage radius of femtoBS j) **then**
25: $\quad\quad\quad\quad\quad\quad\quad\quad\quad$ Initiate handover of the interfering femtoUE to femtoBS j
26: $\quad\quad\quad\quad\quad\quad\quad$ **else**
27: $\quad\quad\quad\quad\quad\quad\quad\quad\quad$ Occupy the next sub-carrier within S_{fi}
28: $\quad\quad\quad\quad\quad\quad\quad\quad\quad$ **Goto** *Stage 2a*
29: $\quad\quad\quad\quad\quad\quad\quad$ **end if**
30: $\quad\quad\quad\quad\quad$ **end if**
31: $\quad\quad\quad$ **end while**
32: *Stage 2b* $\quad\quad\quad\quad\quad\quad\quad\quad$ {no more free sub-carriers in current outer region sub-band}
33: $\quad\quad\quad$ **while** $(S_{fo} = NULL, N_o \ not\ equal\ 0)$ **do**
34: $\quad\quad\quad\quad\quad N_o \quad \leftarrow \ N_o-1;$
35: $\quad\quad\quad\quad\quad S_{fo} \leftarrow (S - S'_{fi})$
36: $\quad\quad\quad\quad\quad S_f^* \quad \leftarrow$ Set of (N_o-1) sub-bands with comparatively higher RSSI value
37: $\quad\quad\quad\quad\quad S_{fo} \leftarrow S_{fo} - S_f^{*}{}'$ $\quad$ {frequency sub- band allocated for femtoBS j}
38: $\quad\quad\quad\quad\quad$ **if** $(SINR_{UL\_Fo}$ at femtoBS j on occupied sub-carrier within $S_{fo} < T$ for $t > \tau_l)$ **then**
39: $\quad\quad\quad\quad\quad\quad\quad$ Decrease transmit power of femtoUE attached to femtoBS j by δ
40: $\quad\quad\quad\quad\quad$ **end if**
41: $\quad\quad\quad\quad\quad$ **if** $(SINR_{UL\_Fo}$ at femtoBS j on occupied sub-carrier within $S_{fo} < T$ for $t > \tau_2)$ **then**
42: $\quad\quad\quad\quad\quad\quad\quad$ **if** (interfering femtoUE within coverage radius of femtoBS j) **then**
43: $\quad\quad\quad\quad\quad\quad\quad\quad\quad$ Initiate handover of the interfering femtoUE to femtoBS j
44: $\quad\quad\quad\quad\quad\quad\quad$ **else**
45: $\quad\quad\quad\quad\quad\quad\quad\quad\quad$ Occupy the next sub-carrier within S_{fo}
46: $\quad\quad\quad\quad\quad\quad\quad\quad\quad$ **Goto** *Stage 2b*
47: $\quad\quad\quad\quad\quad\quad\quad$ **end if**
48: $\quad\quad\quad\quad\quad$ **end if**
49: $\quad\quad\quad$ **end while**
50: **end for**

experienced. Here A′ corresponds to the reversed UL and the DL carriers of sub-band A; which is used by femtoUEs in the cell-edge regions (E1–E6). Similar is the case for other sub-bands as well i.e. B′, C′, D′, E′, F′ and G′ are used by the femtoUEs in the cell-center regions (C1–C6). Selection of frequency sub-band by the femtoBS is based on the assumption that the separating distance between the base stations on either tier are significantly large so that the interference is within tolerable limits. In addition to this, the smaller transmission range of femtoBS in the cell-edge region assures that the macroUEs operating on the same sub-band in the cell-center region as well as in the neighboring macrocell are free from interference.

To sum up, the intra-cell interference is mitigated since the cell-center UEs do not share the same spectrum with cell-edge UEs and inter-cell interference is minimized due

to the spatially separated frequency allocation with orthogonal polarization. Also the inter-tier interference is controlled since the UEs in both tiers make use of different spectrum in a given zone that too in reversed mode.

3.5 Self-optimization by femtoBS

The key issue that self-optimization phase addresses is the dynamic selection of additional frequency spectrum considering the effect of co-channel and co-tier interference in a heavy traffic environment. Since frequency resources are limited, it is important to enable efficient frequency reuse while satisfying the bandwidth requirements. In the current scenario, even though the frequency reuse is enabled via proper geographic separation, the possibilities of bandwidth scarcity cannot be neglected completely. As a result fairness measures are applied by the FMS to optimize the network performance by ensuring that every sector is allotted sub-carriers based on its user density and the corresponding QoS requirements. The resource allocation and QoS information recovered by the femtoBS from the FMS through the femto-gateway enables it to adopt a throughput constrained opportunistic scheduling [31]. During every periodic cycle of status update from the femtoBSs, FMS determine the sectors which are lacking in spectral resources to satisfy their required QoS. On finding such sectors, immediate actions are taken by the FMS to initiate the femtoBS to aggressively access additional sub-bands (and hence sub-carriers) from the macrocell spectrum adhering to the condition that the resulting aggregated cross-tier interference is constrained and maintained within acceptable limits.

Stage 2a and 2b of the operational algorithm explains how the additional sub-bands and hence sub-carriers are accessed one after the other by the femtoBS in the inner region and outer region respectively. After accessing a new sub-band, in case the SINR at a femtoUE operating along a given sub-carrier falls below a pre-determined threshold T for a time interval τ_1 the self-optimization feature adopts the first countermeasure of decrementing the femtoBS transmit power by a value δ. This triggers a similar reaction from the interfering femtoBS as well, which will limit the overall interference and hence improve the SINR. If the femtoUE still reports a low value for SINR, the femtoBS waits for a time interval τ_2 and determines whether the UE attached to the interfering femtoBS is within its own coverage area. If within its radio transmission range, the femtoBS initiates a handover for this UE, and accepts it as its own registered user. If the UE is out of its coverage area, the femtoBS chooses the next sub-carrier within the selected sub-band for its operation and repeat these steps until it becomes capable of transmitting with the guaranteed QoS. The introduction of timeouts τ_1 and τ_2 help in avoiding unnecessary handovers due to channel fluctuations or presence of fast-moving UEs within the femtoBS coverage area. This dynamic access of spectrum satisfies the lower capacity bound of every attached user, before additional sub-carriers are allocated to achieve maximum gain for users with better channel quality. When the same scheduling strategy is applied at the macroBS, the problem of lower throughput for the cell-edge region users can be solved to an extend by imposing higher value for their lower bounds which always gets satisfied before serving cell-center region users. In short, the algorithm assures bandwidth efficiency with the guarantee that the process does not exacerbate the interference in the network.

In addition to this, the self-optimization feature also optimizes the transmission characteristics of femtocells for which a combination of co-channel reuse with orthogonal allocation is introduced. The use of cross-polarized transmission is considered as a means of eliminating the cross-tier interference and thereby increase the SINR. For this purpose, circular cross-polarization is chosen as the best mode of transmission in wireless network as explained before. Since the transmission along all the sub-bands in the macrocell network is enabled through left hand circular polarization (LHCP), the spectrum allocated to the randomly distributed femtocells, will make use of a polarization orthogonal to that of the macrocell network i.e. right hand circular polarization (RHCP) as explained in Fig. 2. The sense of rotation being orthogonal to each other ensures isolation and cannot be altered even with random fluctuations or phase changes. This is because other than for any meta-material, no naturally existing substance has negative permeability or permittivity [32]. The different orthogonal polarization states (LHCP and RHCP) of a given frequency can be depicted using a Poincare sphere [33]. Two points on the surface of the Poincare-sphere are orthogonally polarized if the line joining them passes through the center of the sphere and is cross polarized if they are symmetrically placed with respect to the equator of the sphere. This property makes it possible for the same frequency to be allocated to femtocell users and macrocell users simultaneously with orthogonal/cross polarization. In short, co-existing femtocell and macrocell users make use of orthogonal/alternate polarization so as to maximize the isolation between their transmissions and hence increase the communication quality.

3.6 Self-healing by femtocells

In the case of any sudden variations in the network configuration, the self-healing phase try to bring the system to a stable state without compromising on the QoS requirements. It enables the automatic detection and resolution of failures and reconfigures the current

settings to facilitate the smooth functioning of two-tier network with minimal impact on each other. When the failure is resolved, it gets back to its normal settings. The self-healing phase also takes care of the polarization changes during the handover procedures when a UE switches from a macrocell network to a femtocell network and vice versa.

4 System analysis

Metrics play a significant role in multi-tier systems where the channel conditions are varying, traffic load is unpredictable and users in each tier have individual priorities to satisfy. For example, macrocell systems with heavy traffic load will have to optimize spectral efficiency whereas femtocell systems that guarantee better QoS will have to ensure high data-rate to its customers. Since optimizing one metric may result in sub-optimal performance of other metrics, designers usually come up with a hierarchy for the priorities, then fix thresholds for multiple metrics so as to ensure better service in each tier. This section discuss about such metrics and the corresponding thresholds that play a primary role in improving the overall system performance.

An OFDMA downlink cellular scenario with two tiers corresponding to macrocell network and femtocell network is considered as the system model. The basic radio resource unit that can be allocated in OFDMA transmission is a physical resource block (PRB). Intra-cell interference reduction is guaranteed by scheduling at most one UE per PRB in each cell [34–35]. The network is composed of seven macrocells with macroUEs uniformly distributed and femtoUEs randomly deployed. The sub-carriers from the designated frequency sub-bands as in Fig. 5 are allocated to the macroUEs which trigger the femtoBSs to select its own operational frequency owing to minimal interference [24]. Now, let P_{fb}, P_{fu},P_{mb} and P_{mu} represent the transmit powers of the femtoBS, femtoUE, macroBS and macroUE respectively, S_{Mi}, S_{Fi} and $S_{Mo}S_{Fo}$ represent the bandwidth allotted to the macroUEs and femtoUEs in the inner region and outer region respectively, σ^2 represents the noise power spectral density, P_s^{rc} corresponds to the transmitted signal power from sender s to receiver rc, d denotes the random variable which represents the distance between the interfering BS and the UE under consideration, n represents the path loss exponent and $|h_0|^2$ represent the small scale fading between any BS under consideration and the attached UE. Because the bandwidth and time duration of PRB are restricted [36], it is assumed that all sub-carriers within a PRB experience the same log-normal shadowing and frequency-flat Rayleigh fading [34]. In addition, the shadowing and fading coefficients remain constant within

each PRB [37], but may vary from one PRB to the next. Hence the interference power at a receiver is assumed to be the sum of received power from all other base stations making use of the same sub-carrier as that of the home base station and is assumed to follow a general statistical distribution that includes all random effects like fading, shadowing etc.

4.1 Sub-carrier allocation

Using Monte-Carlo simulations, it is shown in [38] that, the average network throughput is maximized when the sub-carrier allocation between the cell-center and cell-edge users is proportional to the square of the ratio of the inner region radius [αR where $\alpha \, \epsilon \, (0, 1)$] to the macrocell radius (R). Hence the ratio of the sub-carrier allocation (k) between the inner and the outer region of a macrocell network can be expressed as a factor of the area occupied and is given by:

$$k = \frac{\alpha^2}{1 - \alpha^2} \tag{3}$$

Thus the total number of available sub-carriers is subdivided into $S_1 = [S \, \alpha^2] \, (\sim A)$ and $S_2 = S - S_1$ and allotted among the macroUEs in the cell-center and cell-edge region respectively. S_2 is further partitioned into subbands $\sim (B, C, D, E, F, G)$ and allotted to macroUEs in 6 zones within the cell-edge region as shown in Fig. 5. Now as per the proposed scheme, the number of sub-carriers available to the femtocell users is expected to be the same as the macrocell users. Also, twice the frequency spectrum is available for resource allocation with macrocell operating on the conventional frequency bands and femtocell operating on the reversed frequency bands. Thus sub-carrier allocation is reversed for femtoUEs with $S_1' = (\sim A')$ and $S_2' = S - S_1'$ made available to femtoUEs in the cell-edge and cell-center region respectively. S_{Fi} is further divided into sub-bands $\sim (B', C', D', E', F', G')$ and allotted to femtoUEs in six sectors within the cell-center region as the operational algorithm explained in Table 1. From these equations, it can be concluded that one of the main advantage of using the RFA scheme is the ability to achieve 100 % allocation within each cell as well as each tier.

4.2 Power allocation

The cell-edge (outer) macroUEs will require higher power allocation compared to cell-center (inner) macroUEs, if it is in case of conventional cellular architecture. However, such networks results in inter-cell interference. As a potential solution to this problem, in CPCFA scheme the overall transmit power is reduced and inter-cell interference is controlled through the use of DAS which possess

the additional merit of better and efficient coverage along with extended battery life [39]. This assures efficient interference-limited transmission in the cell-edge region as well. Assuming the total transmitting power (P_t) to be evenly distributed among all the sub-carriers (or PRBs) within the cell-center and cell-edge region of the macro-cell, with P being the power per PRB (the power consumption per PRB is assumed to be equal for the sake of fair comparison) and S being the total available bandwidth, we have:

$$PS\left(\frac{k}{1+k}\right) + \sum_{i=1}^{6} P_i = P_t \tag{4}$$

Here $\sum_{i=1}^{6} P_i = PS\left(\frac{1}{1+k}\right)$, where P_i corresponds to the transmit power from the DAE i. It is evident that the factors P_i, α and k has a critical impact on the performance of the system. Variation in service distribution in each cell can be ensured by adjusting the value of α. With increase in α the cell-center region radius increases, which results in more PRBs or sub-bands to be allocated to the cell-center region UEs and hence increase their average throughput. The reverse happens for decrease in α value, resulting in an improved throughput for the cell-edge region UEs. The capacity of the cell-edge region is also dependent on transmit power P_i. In short, the implementation of DAS helps in maintaining an optimal value for UE performance. Selecting an appropriate value for α and hence that of k based on the system preferences helps in improving the overall performance by imposing a strict control over the interference and thereby improves the average user throughput.

4.3 Throughput

The average received power at the femtoUE in the downlink is given by:

$$P_{avg} = P_{fb}I \tag{5}$$

$$P_{avg} = P_{fb}|h_0|^2 d^{-n} \tag{6}$$

where d is the distance between the femtoBS and the femtoUE and I represents the channel attenuation. With reverse frequency allocation, the associated SINR at a femtoUE in the downlink is formulated as:

$$SINR_{DL\_Fi} = \frac{P_i^l|h_0|^2 d^{-n}}{\sum_{j=1,j\neq i}^{Fi} P_{fb}I_j^l + \sum_{k=1}^{Mo} P_{mu}I_k^l + \sigma^2} \tag{7}$$

$$SINR_{DL\_Fo} = \frac{P_i^l|h_0|^2 d^{-n}}{\sum_{j=1,j\neq i}^{Fo} P_{fb}I_j^l + \sum_{k=1}^{Mi} P_{mu}I_k^l + \sigma^2} \tag{8}$$

where $SINR_{DL\_Fi}$ is the signal to interference plus noise ratio at the inner region femtoUE, $SINR_{DL\_Fo}$ is the signal

to interference plus noise ratio at the outer region femtoUE, $I_j^l = \left|h_j^l\right|^2 d^{-n}, I_k^l = \left|h_k^l\right|^2 d^{-n}$. The interference at femtoUE l is due to the DL signal transmission from femtoBS (j) and UL signal transmission from macroUE (k) which are using the same frequency band as that of femtoUE l. As evident from (7) and (8), unlike the classical fractional frequency reuse systems, the femtoUEs in the inner region is interfered only by femtoBSs located in the inner region and is never subjected to interference by transmissions from femtoBSs located in the outer region.

Further employment of polarimetric dimension to ensure orthogonal allocation of spectrum across tiers, assures significant capacity improvement by means of efficient interference control. In this case, the set of interfering BSs are assumed to use the same co-polar sub-carrier within the same tier but with orthogonal polarization in different tier. It is for this reason that femtocell network adopts RHCP for its transmission whereas the macrocell network employs the orthogonal LHCP for its transmission. While making use of cross polarized signals for transmission in femto-macro networks, with P_s^{rc} representing the average power received at receiver rc when transmitted from sender s, it is depicted in terms of the XPD value based on the signal polarization as [40]:

$$\begin{aligned} &\text{For cross-polarized reception: } \frac{1}{XPD}P_s^{rc} \\ &\text{For co-polarized reception: } \frac{XPD-1}{XPD}P_s^{rc} \end{aligned} \tag{9}$$

Taking specifically the case of femto-macro network, femtocells are assumed to have co-polar transmissions whereas macrocells resort to cross-polar transmission with respect to the femto-user under consideration. Hence applying the polarimetric orthogonality in Eqs. (9)–(7) and (8) yields DL SINR as:

$$SINR_{DL\_Fi} = \frac{P_i^l|h_0|^2 d^{-n}(XPD-1)}{\sum_{j=1,j\neq i}^{Fi} P_{fb}^{||}(XPD-1) + \sum_{k=1}^{Mo} P_{mu}^{\perp} + \sigma^2} \tag{10}$$

$$SINR_{DL\_Fo} = \frac{P_i^l|h_0|^2 d^{-n}(XPD-1)}{\sum_{j=1,j\neq i}^{Fo} P_{fb}^{||}(XPD-1) + \sum_{k=1}^{Mi} P_{mu}^{\perp} + \sigma^2} \tag{11}$$

where $P_{fb}^{||}\left(= P_{fb}|h_0|^2 \left(d_{fb}^{fu}\right)^{-n}\right)$ is the interference at femtoUE l due to the DL signal transmission from femtoBS j and $P_{mu}^{\perp}\left(= P_{mu}|h_0|^2 \left(d_{mu}^{fu}\right)^{-n}\right)$ is the interference at femtoUE l due to the UL signal transmission from macroUE k. The Shannon-Hartley bound [41] is further used to calculate the maximum amount of error-free digital data that can be transmitted over the communication link with a specified bandwidth. Equations (10) and (11) highlight that cross-polarized transmission can be utilized as an effective

measure to improve the downlink system capacity of the femto-macro network that employs the CPCFA scheme, if one tier makes use of a polarization orthogonal to that of the other tier which in turn depends on the cross-polarization discrimination maintained between the two tiers. In addition to this, adoption of CPCFA proves to be a promising practical solution to minimize the chances of interference to the macrocell network as well, which can be demonstrated in terms of primary protection ratio (PPR). Taking $PPR = \frac{c_{macro+femto}}{c_{macro\_only}}$ where $C_{macro+femto}$ being the capacity of the macroUEs in the presence of interference from the femtoUEs, and C_{macro_only} being the capacity of the macroUEs without any interference [42], CPCFA seems to offer significantly higher value for PPR.

4.4 Coverage probability

Coverage probability definitely decreases with increase in interference from the nearby radio transmissions which include femtocells, overlaid macrocell, and neighboring macrocells. Coverage probability analysis of the CPCFA scheme can project a clear picture on the probability of successful transmission. A node is said to be in coverage, or the transmission from a femtoBS to a femtoUE is considered successful if and only if the SINR is above a threshold say T. This threshold value definitely depends on the receiver's characteristics like sensitivity, modulation, coding scheme etc. Let the traffic at the interfering femtoBSs and macroBSs be modeled by a sequence of independent indicators with for all i, $\Lambda_i \, \varepsilon \{0,1\}$ such that $\mathbb{P}\{\Lambda_i = 1\} = \Lambda$ and $\mathbb{P}\{\Lambda_i = 0\} = 1 - \Lambda$ Thus the coverage probability for the femtocell downlink in the inner region (P_{c_i}) is expressed as :

$$
\begin{aligned}
P_{c\_i} &\triangleq \mathbb{P}(SINR_{DL\_Fi} > T) \\
&= \mathbb{E}_{P_{int\_DL}}[\mathbb{P}(SINR_{DL\_Fi} > T)|P_{int\_DL}]
\end{aligned}
\tag{12}
$$

$$
= \mathbb{E}\left[exp\left(\frac{-T}{Pd^{-n}(XPD-1)} \left(\sum_{j=1, j\neq i}^{Fi} P_{fb}^{\|}\Lambda_j(XPD-1) + \sum_{k=1}^{Mo} P_{mu}^{\perp}\Lambda_k + \sigma^2 \right) \right) \right]
\tag{13}
$$

$$
= exp\left(\frac{-T\sigma^2}{Pd^{-n}(XPD-1)} \right) \times \mathbb{E}\left[\prod_{j=1, j\neq i}^{Fi} exp\left(\frac{-TP_{fb}^{\|}\Lambda_j}{Pd^{-n}} \right) \right]
$$

$$
\times \mathbb{E}\left[\prod_{k=1}^{Mo} exp\left(\frac{-TP_{mu}^{\perp}\Lambda_k}{Pd^{-n}(XPD-1)} \right) \right]
\tag{14}
$$

The expectation in the last term of (14) can be expressed as:

$$
\begin{aligned}
\mathbb{E}\left[exp\left(\frac{-TP_{fb}^{\|}\Lambda_j}{Pd^{-n}} \right) \right] &= \mathbb{P}(\Lambda_j = 1)x \int_0^{\infty} exp\left(-\frac{TP_{fb}}{Pd^{-n}} \right) \\
&\quad f_{p_{fb}^{\|}}(p_{fb})dp_{fb} + \mathbb{P}(\Lambda_j = 0)x1 \\
&= 1 - \frac{T\Lambda}{\left(\frac{P}{P_{fb}^{\|}}\right)\left(\frac{d}{d_{fb}^{fu}}\right)^{-n} + T}
\end{aligned}
\tag{15}
$$

The expectation in the last term of (14) can be expressed as:

$$
\begin{aligned}
\mathbb{E}\left[exp\left(\frac{-TP_{mu}^{\perp}\Lambda_j}{Pd^{-n}(XPD-1)} \right) \right] &= \mathbb{P}(\Lambda_k = 1) \\
\times \int_0^{\infty} exp\left(-\frac{TP_{mu}}{Pd^{-n}(XPD-1)} \right) f_{p_{mu}^{\perp}}(p_{mu})dp_{mu} &+ \mathbb{P}(\Lambda_k = 0) \times 1 \\
= 1 - \frac{T\Lambda}{(XPD-1)\left(\frac{P}{P_{mu}^{\perp}}\right)\left(\frac{d}{d_{mu}^{fu}}\right)^{-n} + T}
\end{aligned}
$$
$$
\tag{16}
$$

Substituting (15) and (16) in (14), yields coverage probability of inner region femtocell in the downlink as:

$$
\begin{aligned}
P_{c\_i} &= exp\left(\frac{-T\sigma^2}{Pd^{-n}(XPD-1)} \right) \\
&\times \prod_{j=1, j\neq i}^{Fi}\left\{ 1 - \frac{T\Lambda}{\left(P_{fb}^{\|}\right)\left(\frac{d}{d_{fb}^{fu}}\right)^{-n} + T} \right\} \\
&\times \prod_{k=1}^{Mo}\left\{ 1 - \frac{T\Lambda}{(XPD-1)\left(\frac{P}{P_{mu}^{\perp}}\right)\left(\frac{d}{d_{mu}^{fu}}\right)^{-n} + T} \right\}
\end{aligned}
\tag{17}
$$

Similarly, the coverage probability for the outer region femtocell in the downlink (P_{c_o}) is expressed as:

$$
\begin{aligned}
P_{c\_o} &= exp\left(\frac{-T\sigma^2}{Pd^{-n}(XPD-1)} \right) \\
&\times \prod_{j=1, j\neq i}^{Fo}\left\{ 1 - \frac{T\Lambda}{\left(\frac{P}{P_{fb}^{\|}}\right)\left(\frac{d}{d_{fb}^{fu}}\right)^{-n} + T} \right\} \\
&\times \prod_{k=1}^{Mi}\left\{ 1 - \frac{T\Lambda}{(XPD-1)\left(\frac{P}{P_{mu}^{\perp}}\right)\left(\frac{d}{d_{mu}^{fu}}\right)^{-n} + T} \right\}
\end{aligned}
\tag{18}
$$

Coverage probability analysis definitely provides interesting insights on the expected system performance. The first term on the right hand side of (17) and (18) is relevant only in systems where the throughput is limited by the background noise in comparison to the interference from neighboring nodes. However, in dense multi-cell, muti-tier networks where the background noise is negligible when compared to the interference, the transmission is limited by the interference and polarization terms (i.e. the second and

third terms in the expression) which depends on the polarization characteristics of the interferers, traffic distribution and network topology.

4.5 Maximum permissible active femtocell density

When the femto-macro network shares the radio spectrum, and co-channel reuse is permissible within the system, there is always a maximum active femtocell density beyond which every single addition in the femtoBS density increases the interference to the macrocell network. When the femtoUE reuses the frequency sub-band of the macroBS in the downlink, the received SINR highly depends on its distance from the serving femtoBS and the interfering macroUE. The interference statistics measured by a

With λ representing the spatial density of the femtoUEs, the moment generating function of I_{fb}^{fu} is given by [43]:

$$
\mathbb{E}\left[exp\left(-sI_{fb}^{fu}\right)\right] = exp\left(-2\pi\lambda \int_0^\infty \frac{u}{1 + \frac{u^n}{sP_{fb}}} du\right)
$$

$$
= exp\left(-\lambda(sP_{fb})^{\frac{2}{n}}K\right) \tag{20}
$$

where $K = \dfrac{2\pi^2}{n\sin\left(\frac{2\pi}{n}\right)}$

In the CPCFA system, to guarantee the outage of a femtoUE due to cross-tier interference, it is positioned at the coverage boundary of its serving femtoBS with shortest distance to the interfering macroUE. We have from the previous section,

$$
P_{c\_i} \triangleq \mathbb{P}(SINR_{DL\_Fi} > T) = \mathbb{P}\left(\frac{P_i^l|h_0|^2 d^{-n}(XPD-1)}{\sum_{j=1}^{Fi} P_{fb}|h|^2\left(d_{fb}^{fu}\right)^{-n}(XPD-1) + \sum_{k=1}^{Mo} P_{mu}|h|^2\left(d_{mu}^{fu}\right)^{-n} + \sigma^2} > T\right)
$$

$$
= \mathbb{E}\left[exp\left(\frac{-T}{Pd^{-n}(XPD-1)}\left(\sigma^2 + \sum_{k=1}^{Mo} P_{mu}\left(d_{mu}^{fu}\right)^{-n}\Lambda_k + \sum_{j=1,j\neq i}^{Fi} P_{fb}\left(d_{fb}^{fu}\right)^{-n}\Lambda_j(XPD-1)\right)\right)\right] \tag{21}
$$

femtoUE is a representative of that experienced by all other femtoUEs [40]. From (10) and (11), the interference experienced at a femtoUE l in the inner region and outer region respectively due to the downlink transmissions along the same frequency sub-band used by nearby femtoBS j is given by :

For inner region : $I_{fb}^{fu} = \sum_{j=1,j\neq i}^{Fi} P_{fb}|h_0|^2\left(d_{fb}^{fu}\right)^{-n}$

For outer region : $I_{fb}^{fu} = \sum_{j=1,j\neq i}^{Fo} P_{fb}|h_0|^2\left(d_{fb}^{fu}\right)^{-n}$ $\qquad (19)$

From (16) and (20), (21) becomes:

$$
P_{c\_i} = exp\left(\frac{-T\sigma^2}{Pd^{-n}(XPD-1)}\right)
$$
$$
\times \prod_{k=1}^{Mo}\left\{1 - \frac{T\Lambda}{(XPD-1)\left(\frac{P}{P_{mu}^\perp}\right)\left(\frac{d}{d_{mu}^{fu}}\right)^{-n} + T}\right\}
$$
$$
\times \left\{exp\left(-\lambda_i T^{\frac{2}{n}}K\Lambda(XPD-1)d^2\right)\right\} \tag{22}
$$

where λ_i is the maximum permissible femtoBS density in the inner region which is given by:

$$
\lambda_i = \frac{-\ln\left[P_{c\_i}\left(\prod_{k=1}^{Mo}\left\{1 - \frac{T\Lambda}{(XPD-1)\left(\frac{P}{P_{mu}^\perp}\right)\left(\frac{d}{d_{mu}^{fu}}\right)^{-n} + T}\right\}\right)^{-1}\right] + \left(\frac{-T\sigma^2}{Pd^{-n}(XPD-1)}\right)}{\left(T^{\frac{2}{n}}K\Lambda(XPD-1)d^2\right)} \tag{23}
$$

Similarly, the maximum permissible femtoBS density in the outer region is given by:

$$\lambda_o = \frac{-\ln\left[P_{c\_o}\left(\prod_{k=1}^{Mi}\left\{1 - \frac{T\Lambda}{(XPD-1)\left(\frac{P}{P_{mu}^\perp}\right)\left(\frac{d}{d_{mu}^{fu}}\right)^{-n}+T}\right\}\right)^{-1}\right] + \left(\frac{-T\sigma^2}{Pd^{-n}(XPD-1)}\right)}{\left(T^{\frac{2}{n}}K\Lambda(XPD-1)d^2\right)} \tag{24}$$

4.6 Average system sum rate in downlink

The maximum achievable downlink capacity for a femtoUE j on a sub-carrier s is given by:

$$C_{j\in Fi}^s = \Delta B \log_2(1 + \gamma SINR_{DL\_Fi}) \tag{25}$$

$$C_{j\in Fo}^s = \Delta B \log_2(1 + \gamma SINR_{DL\_Fo}) \tag{26}$$

where ΔB corresponds to the sub-carrier spacing, γ is a constant defined by $-1.5/\ln(5\times BER)$ where BER represents the target bit error rate (e.g.,10^{-6}) [24]. Similarly, the maximum achievable downlink capacity for a macroUE k on a sub-carrier s is given by:

$$C_{k\in Mi}^s = \Delta B \log_2(1 + \gamma SINR_{DL\_Mi}) \tag{27}$$

$$C_{k\in Mo}^s = \Delta B \log_2(1 + \gamma SINR_{DL\_Mo}) \tag{28}$$

where $SINR_{DL\_Mi} = \dfrac{P_i^l|h_0|^2 d^{-n}(XPD-1)}{\sum_{j=1,j\neq i}^{Fo}P_{fu}^{\|}+\sum_{k=1}^{Mi}P_{mb}^\perp(XPD-1)+\sigma^2}$ and

$$SINR_{DL\_Mo} = \frac{P_i^l|h_0|^2 d^{-n}(XPD-1)}{\sum_{j=1,j\neq i}^{Fi}P_{fu}^{\|}+\sum_{k=1}^{Mo}P_{mb}^\perp(XPD-1)+\sigma^2}$$

Here $SINR_{DL\_Mi}$ is the signal to interference plus noise ratio of the inner region macrocell and $SINR_{DL\_Mo}$ is the signal to interference plus noise ratio of the outer region macrocell. The average system sum rate C_{avg} is given by [12]:

$$\begin{aligned}C_{avg} &= \frac{\sum_{j\in F_i}\sum_{s\in S}\chi_{j\in F_i}^s C_{j\in F_i}^s}{F_i} + \frac{\sum_{j\in F_o}\sum_{s\in S}\chi_{j\in F_o}^s C_{j\in F_o}^s}{F_o}\\ &+ \frac{\sum_{k\in M_i}\sum_{s\in S}\chi_{k\in M_i}^s C_{k\in M_i}^s}{M_i}\\ &+ \frac{\sum_{k\in M_o}\sum_{s\in S}\chi_{k\in M_o}^s C_{k\in M_o}^s}{M_o}\end{aligned} \tag{29}$$

where in general $\chi^s = 1$ when a sub-carrier s is allocated to a UE, otherwise it is set to 0.

4.7 Interference free femtocell exclusive region (IFFER)

In addition to having a proper coverage, the derivation of an interference free femtocell exclusive region (IFFER) would play a key role in the placement of femtoBS in an indoor

environment. This interference free coverage region is usually dependent on parameters like transmit power of the femtoBS and macroBS, distance of the femto-user from the macroBS and femtoBS, path loss exponent etc. As per [44] IFFER is defined as the area within a contour where the received power levels from the femtoBS and macroBS are the same. However in CPCFA case, the main source of interference in the femtocell downlink is from macroUEs rather than from the macroBS. To be specific, the interference is from the UL transmissions of the outer region macroUEs for the inner region femtocell downlink and from the UL transmissions of the inner region macroUEs for the outer region femtocell downlink. Figure 6 explains the variation in IFFER with increasing distance from the macroUE in case of CPCFA scheme. Consider a simple scenario where the femto-user is located at the coordinates (x, y). Let the received signal strength from the cross-polarized macroUE located at (x_1, y_1) be $P^\perp_{mu}$ and that received from the co-polarized femtoBS located at (x_2, y_2) be $P^{\|}_{fb}$. Considering the signal to interference ratio to be 0 dB [45] at the border of the IFFER, it can be written as $P^\perp_{mu} = P^{\|}_{fb}$
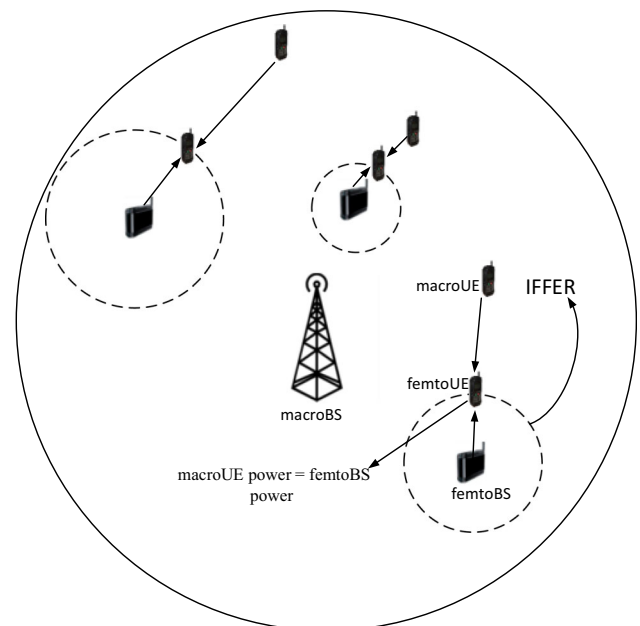

Fig. 6 IFFER in CPCFA scheme

i.e. $P_{mu}|h_0|^2 \left(d_{mu}^{fu}\right)^{-n} = P_{fb}|h_0|^2 \left(d_{fb}^{fu}\right)^{-n}$ $\qquad$ (30)

Applying (9)–(30), results in:

$$\frac{P_{mu}}{XPD\left(d_{mu}^{fu}\right)^n} = \frac{(XPD-1)P_{fb}}{XPD\left(d_{fb}^{fu}\right)^n} \qquad (31)$$

Taking n = 2, and substituting the distance from the macroBS and femtoBS to the femto-user we get:

$$\frac{P_{mu}}{(x-x_1)^2+(y-y_1)^2} = \frac{(XPD-1)P_{fb}}{(x-x_2)^2+(y-y_2)^2} \qquad (32)$$

which can be rearranged and re-written as :

$$x^2 + y^2 + \frac{B_1}{A}x + \frac{B_2}{A}y + \frac{C}{A} = 0$$

where $A = P_{mu} - P_{fb}(XPD-1), B_1 = 2P_{fb}(XPD-1)x_1 - 2P_{mu}x_2, B_2 = 2P_{fb}(XPD-1)y_1 - 2P_{mu}y_2, C = P_{mu}\left(x_2^2+y_2^2\right) - P_{fb}(XPD-1)\left(x_1^2+y_1^2\right)$ However, this denotes the equation of a circle centered at $\left(\frac{-B_1}{2A}, \frac{-B_2}{2A}\right)$ with radius $\sqrt{\frac{B_1^2}{4A^2} + \frac{B_2^2}{4A^2} - \frac{C}{A}}$. Hence IFFER will have an area given by $\pi\left(\frac{B_1^2}{4A^2} + \frac{B_2^2}{4A^2} - \frac{C}{A}\right)$. Thus, it becomes clear that, apart from the location and transmit power of femtoBS, IFFER is dependent on the transmit power of the macroUE and the XPD value too, in a CPCFA network. Higher the XPD between femto-macro transmissions, larger will be the IFFER. For n to be any arbitrary path loss exponent other than 2, the (2/n)-th root needs to be applied to both sides in (30) which becomes exactly similar to the scenario where $n = 2$ with an entirely different value for the transmit powers [44].

5 Results and discussion

In this section CPCFA performance is analyzed and verified through Monte-Carlo simulations in MATLAB environment. Simulation involves an OFDMA cellular scenario with two tiers - macrocell network and femtocell network respectively. The simulation model consider the advantages of the framework developed in [47] which introduces a certain amount of randomness in the model. Hence the macroUEs are uniformly distributed in the network whereas the femtoUEs are randomly placed. The simulation environment assumes the hexagonally-shaped macrocell to be located centrally within a group of 7 macrocells and the central macrocell is assumed to have an omni-directional antenna serving 105 macroUEs with 50 in the cell-center region and 55 in the cell-edge region. Femtocell distribution is varying within this macrocell with a density $\lambda = 1/\left(2500\,\Pi^2\right)$ femtoBS per m^2 with each one having single femtoUE attached to it. The simulation studies

assume a macrocell of radius 600 m. The macrocell radius in the plots also correspond to the mean of the separation between macroBS and the random femtoBS chosen over a series of simulation runs. The non-line of sight path loss variations are tracked according to the channel environment modeled as per wireless world initiative new radio (WINNER) II model [48], and the transmissions are affected by shadowing and a wall loss attenuation of 12 dB. For the polarized transmissions, an XPD value of 10 dB is assumed. We assume a 'snapshot model' for our simulations, where the parameters given in Table 2 are assumed to remain constant over each simulation run [46].

Potential throughput improvement with the CPCFA scheme is analyzed by comparing it with the conventional sectored frequency allocation method (CSFA), the optimal static fractional frequency allocation method (OSFFA) [12], the reverse frequency allocation (RFA) method [14] and the cross-polarized wireless access (CPWA) method [16] as a function of macrocell radius.

Figure 7 projects the comparison of average downlink capacity of femto-macro system for the five different methods as the number of femtoBSs vary within the macrocell with 105 macroUEs. The whopping throughput enhancement with CPCFA strategy is clearly evident from the figure when compared with the other schemes. This is due to reduced co-tier and cross-tier interference, especially for the femtocell users for which the interference from macroBS is completely eliminated. Even though frequency and polarization diversity achieved through RFA and CPWA offers better throughput than OSFFA and

Table 2 MATLAB simulation parameters [46]

| Parameter	Value
Channel bandwidth	10 MHz
Sub-carrier spacing	15 KHz
Carrier frequency	2.5 GHz
Max transmit power of macroBS	43 dBm
Max transmit power of macroUE	23 dBm
Max transmit power of femtoBS	23 dBm
Max transmit power of femtoUE	23 dBm
Thermal noise density	−174 dBm/Hz
Antenna gain of macroBS	15 dBi
Antenna gain of femtoBS	2 dBi
Antenna gain of UE	1 dBi
Inner region radius	450 m
Outer region radius	600 m
Lognormal std. deviation (outdoor)	8 dB
Lognormal std. deviation (indoor)	4 dB
Power decrement δ	3 dB
Threshold for coverage T	10 dB
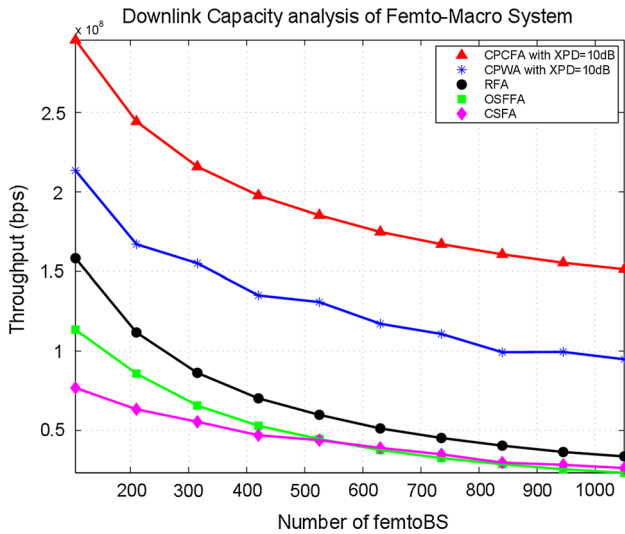
Fig. 7 Downlink capacity analysis of femto-macro system

CSFA, CPCFA guarantees a better system performance by exploiting both of them in a combined fashion. To add on, in comparison to the CPWA, OSFFA and CSFA methods, the increase in usable sub-carriers in the cell-edge and cell-center region for CPCFA strategy, plays a significant role in enhancing the system performance further.

Figure 8 projects the primary protection ratio comparison for the different methods. It is evident from the figure that the legacy macrocell network has the least impact with the incorporation of CPCFA framework. Higher value of PPR is maintained well throughout the macrocell coverage area in case of CPCFA when compared with that of CPWA, RFA, OSFFA and CSFA. Unlike the monotonic trend observed for the CSFA and CPWA methods, a slight variation in PPR is observed towards the boundary of the
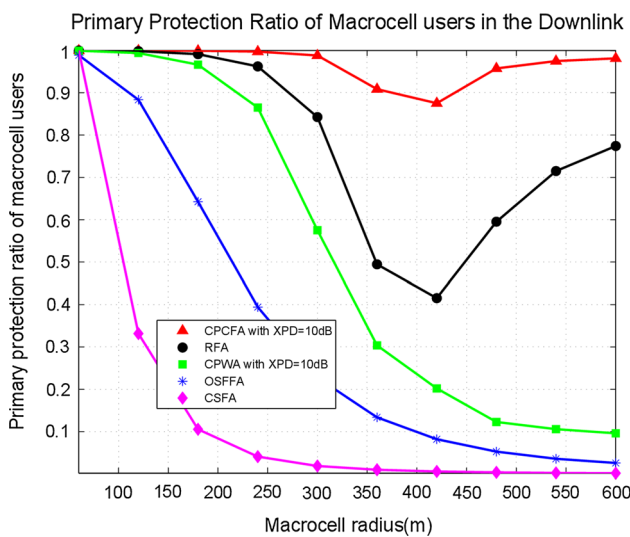
cell-center region due to increase in interference and decrease in macroBS signal strength. However, this is compensated by the incorporation of DAS in the cell-edge region which causes the PPR to attain a comparatively high value towards the cell-edge. This ensures that the incorporation of CPCFA scheme can only result in the betterment of the system performance as a whole with minimal impact on the macrocell network.

Figure 9 compares the coverage probability of different methods. It is clear from the plot that CPCFA scheme offers the highest coverage probability for the femtoUEs throughout the network. The frequency diversity minimizes the interference, while polarization diversity maximizes the co-channel frequency reuse, and hence assures better coverage in CPCFA case. The probability of coverage in case of CPWA and RFA is also comparable to that of CPCFA even though not as high, due to their advantages in terms of frequency diversity and polarization diversity respectively. CSFA and OSFFA has lesser coverage probability in the cell-center region and increases towards the cell edge region. This is because, coverage probability increases as the interference from the macroBS reduces with increase in separation between the femtoUE and the macroBS.

Figure 10 compares the IFFER expansion for different methods along with increase in XPD value. It is evident from the simulation results that with larger XPD, higher is the isolation between the femto-macro network, lesser is the cross-tier interference and hence larger is the IFFER. This siginifies that in a CPCFA network, the IFFER is dependent not only on the transmit powers of the base stations and the path loss exponent but also on the XPD value. This increase in IFFER seems to be almost linear in case of femto-macro network with just reverse frequency
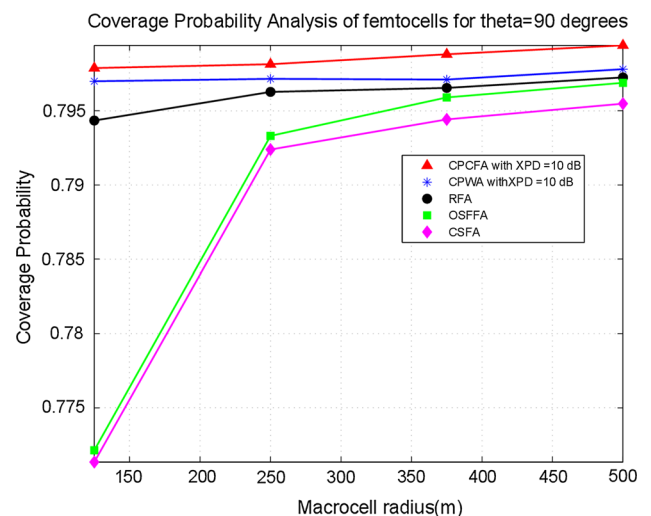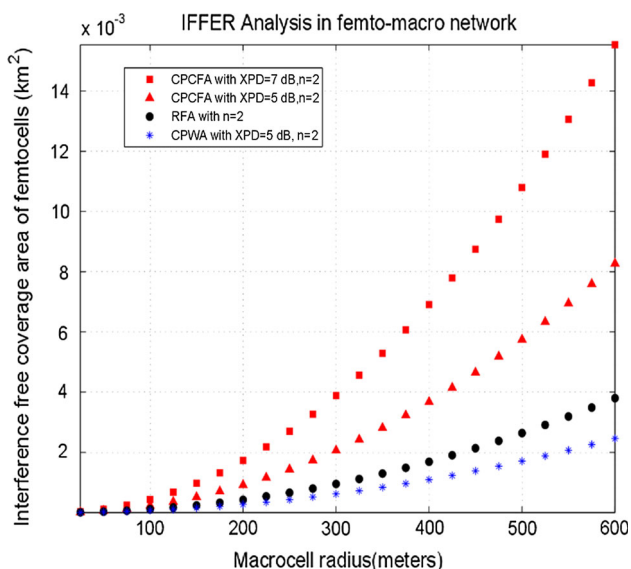

Fig. 8 Primary protection ratio comparison

Fig. 9 Coverage probability analysis

Fig. 10 IFFER analysis

Table 3 Comparison for different system configurations

Average system sum rate comparison (bps)					
User Occupancy	FUE 200	MUE 100	FUE 200	MUE 50	FUE 200	MUE 200
CPCFA					
	1.293×10^7		2.519×10^6		4.688×10^6
CPWA					
	4.464×10^6		9.542×10^6		1.060×10^6
RFA					
	3.413×10^6		6.152×10^5		9.067×10^6
OSFFA					
	2.070×10^6		3.492×10^6		1.115×10^5
CSFA					
	7.882×10^5		9.503×10^5		3.578×10^5

allocation, but exponential when it comes to a two-tier network where isolation is ensured by means of polarization and frequency diversity through CPCFA scheme. Hence CPCFA plays a key role in increasing the coverage area of femtocells and reducing the probability of outage due to sharing of frequency spectrum with the macrocell. Further, the choice of n also proves to be fatal, since increase in n for femtocell network decreases the IFFER whereas increase in n for macrocell network increases IFFER. Hence it becomes the choice of the network operator to have a trade-of between the throughput and coverage probability by manipulating the transmit power and the IFFER. However, the application of cross-polarization together with reverse frequency allocation improves the system performance over these constraints and thereby guarantee the required QoS.

Table 3 projects the improvement in average system sum rate with CPCFA method in comparison to other methods. We find a steady increase in average system sum rate as we move from the CSFA method towards CPCFA method. Further, for different configuration of femto-macro user distribution, CPCFA method steadily guarantees the highest throughput even when we observe slight fluctuations in other schemes. This finally helps to conclude that the CPCFA framework can bring in significant improvement in the downlink system performance and hence serve more data traffic in the downlink.

6 Conclusion

Today, multi-tier heterogeneous networks play a significant role in meeting the coverage and capacity needs of increasingly data centric networks in a cost effective and operationally efficient fashion. However, mass deployment of femtocells within the macrocell network demand the elimination of cross-tier interference problem to prevent performance degradation in the system. In this paper, we have presented a thorough downlink analysis of femto-macro network employing decentralized cross-polarized complementary frequency allocation strategy where self-organizing OFDM femtocells make use of their cognitive capabilities to select their operational frequency based on their location and owing to minimal interference from the macrocell. A theoretical framework exploiting the polarization and frequency diversity to improve the system capacity through frequency reuse has been demonstrated. Eliminating the downlink interference from the macroBS to the femtoBS through CPCFA scheme, enhances the cell-edge user's performance and at the same time control interference in the two tier network with superior spectral efficiency. It has been validated with mathematical analysis and extensive simulation that the system performance can be improved by increasing the XPD value and maintaining the orthogonality of cross polarized signals at 90 degree antenna feed separation. To conclude, even with minor imperfect calibrations, the use of CPCFA in femto-macro network seems to remarkably increase the system capacity and allow efficient frequency reuse in comparison to the eminent fractional frequency reuse methods available in the literature. The present paper primarily focuses on downlink service provisioning and spatial reuse in co-located macro-femto networks with shared spectrum. Nevertheless, much work remains to be investigated on the uplink service provisioning along with user association, the inter-cell interference coordination schemes with dynamic power control to make the frame work more autonomous and scalable; which might be the key to proliferation of this technology on a broader scale.

References

1. Realwireless report for Ofcom, "4G capacity gains, final report," 2011.
2. GPP TR 32.816, Telecommunication management; study on management of Evolved Universal Terrestrial Radio Access Network (E-UTRAN) and Evolved Packet Core (EPC) (Release 8) v1.3.1, 2007.
3. Yavuz, M., Meshkati, F., Nanda, S., Pokhariyal, A., Johnson, N., Roghothaman, B., & Richardson, A. (2009). Interference management and performance analysis of umts/hspa + femtocells. *IEEE Communications Magazine, 47*(9), 102–109.
4. Young, J. S., Hae, G. H., & Kwang, K. S. (2009). "A self organised femtocell for IEEE 802.16e system." In *Proceedings of IEEE Global Telecommunications Conference*, pp. 1–5, December 2009.
5. Berg, J. L. V. D., Litjens, R., Eisenbltter, A., Amirijoo, M., Linnell, O., Blondia, C., et al. (2008). Self-organisation in future mobile communication networks. *ICT - Mob Summit, Sweden, 2,* 915–920.
6. Zetterberg, K., Scully, N., Turk, J., Jorguseski, L., & Pais, A. (2010). "Controllability for self-optimisation of home enodebs," COST 2100, Joint Workshop COST 2100 SWG 3.1 and FP7-ICT-SOCRATES, Greece, February 2010.
7. I. Balan, "Self-optimisation in 3gpp lte networks," Dec., 2009.
8. Aldaya, I., Campuzano, G., Gosset, C., Giacoumidis, E., Doran, N. J., Mikroulis, S., & Castanon, G. (2013). "Novel cost-effective PON-to-mm-wave RoF photonic bridge for multigigabit access networks." In *Proceedings of International Conference on Transparent Optical Networks (ICTON)*, pp.1–4, June 2013.
9. Lopez-Perez, D., Roche, G., Valcarce, A., Juttner, A., & Zhang, J. (2008). "Interference avoidance and dynamic frequency planning for WiMAX femtocells networks." In *Proceedings. of IEEE international conference on communication systems*.
10. Saatsakis, A., Demestichas, P., Merat, V., Page, C. L., Loewel, T., & Nolte, K. (2009). "Femtocell and flexible base station cognitive management." In *Proceedings of IEEE international symposium on personal, indoor and mobile radio communications*, pp. 1–5, September 2009.
11. Lopez-Perez, D., Ladanyi, A., Juttner, A., & Jie, Z. (2009). "OFDMA femtocells: A self-organizing approach for frequency assignment." In *Proceedings of IEEE international symposium on personal, indoor and mobile radio communications*, pp. 2202–2207, September 2009.
12. Saquib, N., Hossain, E., & Kim, D. I. (2013). Fractional frequency reuse for interference management in LTE-advanced hetnets. *IEEE Wireless Communications, 20*(2), 113–122.
13. Jacob, P., James A., & Madhukumar, A. S. (2012). "Downlink capacity improvement and interference reduction through reverse frequency allocation." In *Proceedings of IEEE international conference on communication systems*, pp. 329–333, November 2012.
14. Jacob, P., Madhukumar, A. S., & James, A. (2014). Interference mitigation through reverse frequency allocation in multi-tier cellular network-a downlink perspective. *Wireless Networks-Springer Journal,*. doi:10.1007/s11276-014-0868-x.
15. Jacob, P., Madhukumar, A. S., & Alphones, A. (2013). Interference mitigation through cross polarized transmission in femto-macro network. *IEEE Communication Letters, 17*(10), 1940–1943.
16. Jacob, P., Madhukumar, A. S., & Alphones, A. (2014). Orthogonal circular polarized transmission for interference control in femto-macro networks. *Computer Communications- Special Issue on Networking and Communications for Smart Cities,*. doi:10.1016/j.comcom.2014.09.004dlx.
17. Oestges, C., Erceg, V., & Paulraj, A. (2004) "Propagation modeling of multi-polarized mimo fixed wireless channels", In *IEEE transactions on vehicular technology*, 53(3).
18. Yildirim, F., Sadri, A. S., & Liu, H. (2008). Polarization effects for indoor wireless communications at 60 GHz. *IEEE Communication Letters, 12*(9), 660–662.
19. Rappaport, T. S., & Hawbaker, D. A. (1992). Wide-band microwave propagation parameters using circular and linear polarized antennas for indoor wireless channels. *IEEE Transactions on Communications, 40,* 240–245.
20. Sato, K., Manabe, T., Ihara, T., Saito, H., Ito, S., Tanaka, T., et al. (1997). Measurements of reflection and transmission characteristics of interior structures of office building in the 60-GHz band. *IEEE Transactions on Antennas Propagation, 45,* 1783–1792.
21. Manabe, T., Sato, K., Masuzawa, H., Taira, K., Ihara, T., Kasashima, Y., & Yamaki, K. (1995). Polarization dependence of multipath propagation and high-speed transmission characteristics of indoor millimeter-wave channel at 60 GHz". *IEEE Transactions on Vehicular Technology, 44,* 268–274.
22. Leaves, P., Moessner, K., & Tafazolli, R. (2004). Dynamic spectrum allocation in composite reconfigurable wireless networks. *IEEE Communications Magazine, 42*(5), 72–81.
23. Claussen, H., Ho L., & Samuel, L. (2008). "Self-optimization of coverage for femtocell deployments." In *Proceedings. of the wireless telecomunications symposium (WTS)*, April 2008.
24. Poongup, L., Taeyoung, L., Jangkeun, J., & Jitae, S. (2010) "Interference management in LTE femtocell systems using fractional frequency reuse," In *Proceedings of 12th international conference on advanced communication technology*, vol. 2, pp. 1047–1051, February 2010.
25. CHANG, C. W. W., & Chien-Yuan, C. H. U. (2011) "A high capacity cell architecture based on distributed antenna system and frequency allocation scheme," In *IEICE transactions on communications.*" vol. 94, no. 9, pp. 2690–2695.
26. Zhang, J., Zhang, R., Li, G., & Hanzo, L. (2013). Distributed antenna systems in fractional-frequency-reuse-aided cellular networks. *IEEE Transactions on Vehicular Technology, 62*(3), 1340–1349.
27. Kim, T., Lee, T. (2008). "Throughput enhancement of macro and femto networks by frequency reuse and pilot sensing," In *Proceedings of IEEE International performance, computing and communications conference (IPCCC)*. pp.390–394, December 2008.
28. "IEEE standard for local and metropolitan area networks part 16: Air interface for fixed and mobile broadband wireless access systems." In *IEEE, technology report 802.16*, October 2004.
29. "Radio resource control (RRC); protocol specification, (release 8)," 3GPP technology report Ts 25.331, April. 2008. (Online). http://www.3gpp.org/ftp/Specs/html-info/25331.htm.
30. Bender, P., Black, P., Grob, M., Padovani, R., Sindhushayana, N., & Viterbi, A. (2000). CDMA/HDR: A bandwidth efficient high-speed wireless data service for nomadic users. *IEEE Communications Magazine, 38*(7), 70–77.
31. Ali, S. H., Lee, K. D., & Leung, V. C. M (2009). "Throughput constrained opportunistic scheduling in cellular data networks," In *IEEE transactions on vehicular technology*. vol. 58, pp. 1396–1406.
32. Engheta, N. "Metamaterials with negative permittivity and permeability: Background, salient features, and new trends," In *Proceedings of IEEE MTT-S international microwave symposium digest*. pp. 187–190, June 2003.

33. Cao, B., Zhang, Q. Y., & Jin, L. (2011). Polarization division multiple access with polarization modulation for LOS wireless communications. *EURASIP Journal on Wireless Communications and Networking, 1*, 1–9.

34. Chandrasekhar, V., & Andrews, J. (2009). Spectrum allocation in tiered cellular networks. *IEEE Transactions on Communications, 57*(10), 3059–3068.

35. Andrews, J., Ghosh, A., & Muhamed, R. (2007). Fundamentals of WiMAX: Understanding broadband wireless networking, Prentice Hall.

36. GPP LTE Release 8, http://www.3gpp.org/Release-8.

37. Astely, D., Dahlman, E., Furuskar, A., Jading, Y., Lindstrom, M., & Parkvall, S. (2009). LTE: The evolution of mobile broadband. *IEEE Communications Magazine, 47*(4), 44–51.

38. Bharucha, Z., & Haas, H. (2008). The distribution of path losses for uniformly distributed nodes in a circle. *Research Letters in Communications, 2008*, 1–4.

39. Adachi, F. (2001) "Wireless past and future-evolving mobile communication systems." In *IEICE transactions on fundamentals of electronics communications*, vol. *E84-A*, no.1, pp. 55-60, January 2001.

40. Ntagkounakis, K., Sharif, B., & Dallas, P. (2006). Novel channel and polarization assignment schemes for 2–11 GHz fixed-broadband wireless access networks. *Wireless Personal Communications, 36*(4), 425–443.

41. Shannon, C. E. (1949). Communication in the presence of noise. *Proceedings of the Institute of Radio Engineers, 37*, 10–21.

42. Chatzinotas S., & Ottersten, B. (2012) "Cognitive interference alignment between small cells and a macrocell." In *Proceedings of 19th international conference on telecommunications (ICT), 23–25*. pp.1–6, April 2012.

43. Baccelli, F., Blaszczyszyn, B., & Muhlethaler, P. (2006). An Aloha protocol for multihop mobile wireless networks. *IEEE Transactions on Information Theory, 52*(2), 421–436.

44. Guvenc, I., Jeong, M. R., Watanabe, F., & Inamura, H. (2008). "A hybrid frequency assignment for femtocells and coverage area analysis for co-channel operation." In *IEEE communication letters*, vol. *12*, no. 12, December 2008.

45. Ho L. T. W., & Claussen, H. (2007) "Effects of user-deployed, co-channel femtocells on the call drop probability in a residential scenario," In *Proceedings of IEEE international symposium on personal, indoor and mobile radio communications*. pp. 1–5, September 2007.

46. GPP TS 25.104 V8.10.0, Base station radio transmission and reception (FDD) (2010).

47. Andrews, J. G., Baccelli, F., & Ganti, R. K. (2011). A tractable approach to coverage and rate in cellular networks. *IEEE Transactions on Communications, 59*(11), 3122–3134.

48. WINNER II WP1: WINNER II Part 1 Channel Models. IST-4-027756, D1.1.2, V1.1 (2007).

Ponnu Jacob received her B. Tech. degree from Mahatma Gandhi University, Kerala, India in 2006 and Ph.D. from School of Computer Engineering, Nanyang Technological University, Singapore in 2015. Currently she is working as a Research Fellow with Air Traffic Management Research Institute where she is involved in cognitive spectrum sensing enabled aviation spectrum management research. From 2007 to 2010, she was with Alcatel Lucent Technologies, India where she was involved in W-CDMA research and development activities. Her research interests include wireless communications, heterogeneous networks, interference management and wireless spectrum resource allocation.

A. S. Madhukumar received his B. Tech. degree from College of Engineering, Trivandrum, India, M. Tech from Cochin University of Science and Technology, India and Ph. D. from Department of Computer Science and Engineering, Indian Institute of Technology, Madras, India. He is currently an Associate Professor in the School of Computer Engineering, Nanyang Technological University, Singapore. He was involved in communications and signal processing research at Centre for Development of Advanced Computing, Govt. of India and Institute for Infocomm Research (previously known as Centre for Wireless Communications), Singapore. His current research interests are in heterogeneous networks, cooperative radio systems for mobile multi-hop networks, algorithms and architectures of cognitive radios, new modulation and multiple access schemes, advanced signal processing algorithms for communication systems. He is involved in a number of funded research projects, organizing international conferences, and a permanent reviewer for many internationally reputed journals and conferences. He has published over 200 referred international conference and journal papers. Dr. Madhukumar is a senior member of IEEE.